Picophotonics: Anomalous Atomistic Waves in Silicon

Sathwik Bharadwaj⊙,* Todd Van Mechelen⊙, and Zubin Jacob⊙†

Birck Nanotechnology Center, School of Electrical and Computer Engineering, Purdue University, West Lafayette, Indiana 47907, USA

The concept of photonic frequency-momentum (ω-q) dispersion has been extensively studied in artificial dielectric structures such as photonic crystals and metamaterials. However, the ω-q dispersion of electrodynamic waves hosted in natural materials at the atomistic level is far less explored. Here, we develop a Maxwell Hamiltonian theory of matter combined with the quantum theory of atomistic polarization to obtain the electrodynamic dispersion of natural materials interacting with the photon field. We apply this theory to silicon and discover the existence of anomalous atomistic waves. These waves occur in the spectral region where propagating waves are conventionally forbidden in a macroscopic theory. Our findings demonstrate that natural media can host a variety of yet to be discovered waves with subnanometer effective wavelengths in the picophotonics regime.

I. INTRODUCTION

Functional dependency of the energy and momentum (dispersion) of particles hosted in matter captures the fundamental properties of a material [1]. The dispersion for several electronic, phononic, and magnonic excitations in condensed matter systems [2–16] have been widely studied within an atomistic lattice band theory. However, the concept of frequency and momentum (ω-q) photonic dispersion [17] and the corresponding electromagnetic field confinement [18] have been formulated only in artificial materials such as photonic crystals [19–22], metamaterials [23–25], and other dielectric structures [26,27]. These artificial materials are composed of two or more macroscopic constituents. On the contrary, natural media itself can host electrodynamic waves that adapt the symmetry and periodicity of the material [28,29]. Hence, natural materials can host a variety of yet to be discovered electrodynamic waves and topological photonic properties [29–31]. As such, these are the properties of atomistic matter itself and are not related to a form of macroscopic engineering. In this article, we develop a Maxwell Hamiltonian theory of matter combined with the quantum theory of atomistic polarization to unveil the electrodynamic dispersion of the electromagnetic (photon) field.

Recently, it has been shown that a graphene monolayer in the viscous hydrodynamic state [32] supports spin-1 skyrmions in the bulk and topologically protected electromagnetic edge states at the boundary [31,33,34]. This topological electrodynamic phase of matter is characterized by an optical N invariant [29] fundamentally distinct from the Chern number and $\mathbb{Z}_2$ invariant. The optical N invariant was defined based on a semiclassical hydrodynamic nonlocal (photon momentum $\hbar\mathbf{q} \neq 0$) dielectric response that includes Hall viscosity and the dynamics of electromagnetic waves. However, the Maxwell Hamiltonian theory of matter and the quantum theory of atomistic polarization within the framework of a lattice band theory has not been considered so far. Here, we solve this key challenge and show that the atomistic polarization results in the emergence of a unique class of atomistic waves. In this paper, we apply the theory to silicon (Si), but in the future it can be extended to topological systems with repulsive Hall viscosity.

In Fig. 1, we compare the light-matter interaction theories across varying length scales. The traditional regime of optics and flat metaoptics studies the optical properties within the classical electromagnetism, and the dielectric response is considered to be a material-dependent function. Nanophotonics encompass the study of electromagnetic field interactions in artificial structures such as metamaterials, photonic crystals, and other dielectric structures [35]. Field solutions in these structures can be effectively obtained through a classical wave equation, with the dielectric response dependent on the spatial geometry [36] and frequency. In this article, our focus is picophotonics, which comprises the light-matter interaction in natural materials at the subnanometer regime. We show that in the picophotonic regime, the electromagnetic fields satisfy a picophotonic Bloch functional form. We define the dynamics of the fields by a picophotonic nonlinear eigenvalue equation, which depends on the quantum

---
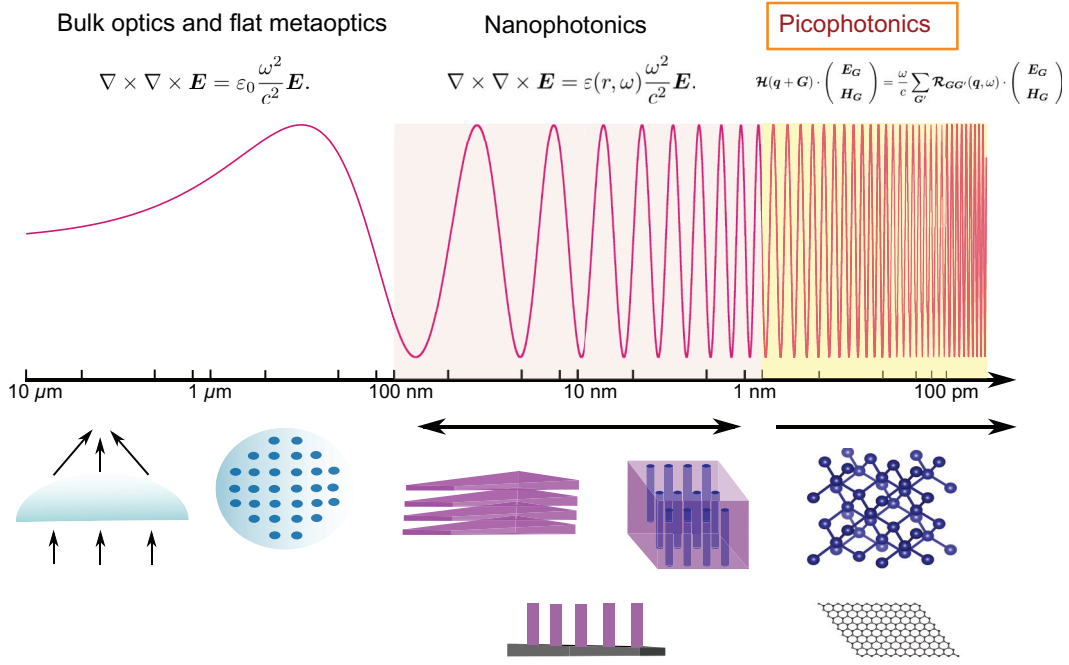*sdaralag@purdue.edu
†zjacob@purdue.edu

FIG. 1.   Branches of optics across the length scales are depicted in the schematic diagram. Bulk optics and flat metaoptics are applicable for electromagnetic waves passing through micrometer-scale artificial structures. Field equations in bulk optics satisfy a standard Maxwell wave equation with a constant dielectric permittivity. Light-matter interaction in metamaterials and photonic crystals are studied within nanophotonics. Field solutions in the nanophotonics regime still satisfy the classical wave equation with possible coupling to hydrodynamic effects. In nanophotonics, the dielectric function may depend on frequency and vary spatially over the region of interest. Here, we define the field of picophotonics, where we analyze the light-matter interaction in natural materials at the subnanometer regime. In this regime of picophotonics, the response function is dependent on the frequency, momentum, and the atomistic local-field effects. The dynamics of electromagnetic waves are studied within the Maxwell Hamiltonian framework along with the quantum theory of atomistic polarization.

theory of atomistic polarization as opposed to semiclassical Drude or hydrodynamic models. Furthermore, we apply this formulation for Si, and discover the existence of anomalous atomistic waves. These waves occur in the frequency range where propagating waves are conventionally forbidden in a macroscopic theory. We show that the anomalous waves observed in Si are highly oscillatory within a unit cell, well within the dominion of picophotonics.

The paper is arranged as follows. In Sec. II, we define the atomistic dielectric tensor and discuss the importance of contributions from the local-field effects in a material. In Sec. III, we derive the transverse atomistic dielectric tensor within a linear response theory. An atomistic nonlocal electrodynamics of matter based on the Maxwell Hamiltonian is described in Sec. IV. In this section, we also define the picophotonic Bloch function and the picophotonic eigenvalue equation for the electrodynamic field. As an application of our formulation, we obtain the nonlocal atomistic dielectric response and the corresponding atomistic electrodynamic dispersion in Si through an isotropic nearly free electron model, as described in Secs. V and VI, respectively. Concluding remarks are presented in Sec. VII.

II. DEFINING THE ATOMISTIC DIELECTRIC TENSOR

In solid-state materials, long-wavelength perturbations can lead to short-wavelength responses due to short-range electronic correlations [37–39]. This phenomenon has been termed the atomistic local-field effect [40]. Consequently, microscopic fields arising from local-field effects vary rapidly within the unit cell. The macroscopic field is obtained through averaging the microscopic fields over a large region compared to the lattice constant. This macroscopic field is not the same as the atomistic electromagnetic field in a material [41]. Inside a material, fields will have rapidly varying terms with wave vector $\mathbf{q} + \mathbf{G}$, where $\mathbf{G}$ is the reciprocal lattice vector and $\mathbf{q}$ is the photon wave vector. Hence, the dielectric response of a material depends on frequency (ω), momentum ($\hbar\mathbf{q}$), and local-field effects. The dielectric response of a material is represented in momentum space as

$$\varepsilon(\mathbf{q} + \mathbf{G}, \mathbf{q} + \mathbf{G}', \omega) \equiv \varepsilon^{\mathbf{G}\mathbf{G}'}(\mathbf{q}, \omega). \qquad (1)$$

When $\mathbf{q} \neq 0$, we obtain the nonlocal dielectric response, and the components with $\mathbf{G}, \mathbf{G}' \neq 0$ are due to atomistic local-field effects. So far, in the literature only the

longitudinal dielectric function (density-density response) $\varepsilon_L^{\mathbf{GG}'}(\mathbf{q}, \omega)$ has been extensively studied [41,42]. However, a crucial gap in the linear response theory of matter is in understanding the influence of local-field effects on the dielectric response arising from a photon field.

Traditionally, electromagnetic properties of matter are treated within a macroscopic local electrodynamic framework, where it is assumed that the dielectric function is only dependent on the frequency $\varepsilon(\omega)$. This consideration is valid only in the long-wavelength limit, $\mathbf{q} \rightarrow 0$. Although there have been efforts to develop quantum electrodynamic first-principles density-functional theory calculations [43,44], applications of such frameworks have been limited to artificial dielectric structures and cavities. These frameworks are also developed in the long-wavelength limit and the photon field is considered to be in vacuum. In this article, our focus is the picophotonic, atomistic regime beyond the cavity quantum electrodynamics [45] and local dielectric response approximations.

For a system with infinitesimal translation symmetry, a jellium model can be used, where we consider a nonlocal dielectric function $\varepsilon(\mathbf{q}, \omega)$ without any contribution from the local-field off-diagonal components. This approximation has been successfully applied for the case of simple metals [46]. The jellium model breaks down in explaining the observed properties of nanoplasmonic structures with metals in the subnanometer domain [47]. Nonlocal quantum effects in nanoplasmonic structures can be explained through hydrodynamic models [48–52] as opposed to a local Drude model response theory. However, as shown in this article, in semiconducting materials, local-field effects beyond the hydrodynamic model take the central role in determining the atomistic electrodynamic dispersion of matter.

Early efforts within classical electrodynamics to include local-field effects in the dielectric function were considered through the Clausius-Mossotti relation (Lorentz-Lorenz equation) [53–55]. In this approximation, the simple cubic lattice of polarizable atomic sites is replaced with a homogeneous cavity. This leads to a connection between the macroscopic dielectric function ε_M in terms of the molecular polarizability [56]. However, the Clausius-Mossotti relation has neither frequency nor momentum dependency on the dielectric function, and does not build in the symmetry of the Brillouin zone of the system. We also note that the widely used approximation of replacing atoms by polarizable harmonic oscillators is confined to the classical regime. Adler [41] and Wiser [42] (from now on termed the Adler-Wiser formulation) put forth the quantum theory of the atomistic longitudinal dielectric function $\varepsilon_L^{\mathbf{GG}'}(\mathbf{q}, \omega)$ based on perturbation theory. Following these efforts, it has been shown that local-field corrections are quintessential to determine the electron self-energy [57–59] and impurity screening potential [60,61]. Here, we introduce the

transverse dielectric function $\varepsilon_T^{\mathbf{GG}'}(\mathbf{q}, \omega)$ going beyond the Adler-Wiser formulation.

III. BEYOND THE ADLER-WISER FORMULATION: ATOMISTIC DIELECTRIC RESPONSE IN MATTER

The Adler-Wiser formulation determines the atomistic longitudinal dielectric response including the local-field effects [41]. This expression for the dielectric function has been the gold standard in first-principles calculations to determine the optical response of a material [62,63]. However, the response of a material to a photon field is determined by the atomistic transverse dielectric tensor. In this section, we develop a quantum theory of $\varepsilon_T^{\mathbf{GG}'}(\mathbf{q}, \omega)$, including local-field effects.

The atomistic dielectric function of a material can be expressed in a longitudinal and transverse basis [41,64,65] as

$$\varepsilon^{\mathbf{GG}'}(\mathbf{q}, \omega) = \begin{bmatrix} \varepsilon_L^{\mathbf{GG}'}(\mathbf{q}, \omega) & \varepsilon_{LT}^{\mathbf{GG}'}(\mathbf{q}, \omega) \\ \varepsilon_{TL}^{\mathbf{GG}'}(\mathbf{q}, \omega) & \varepsilon_T^{\mathbf{GG}'}(\mathbf{q}, \omega) \end{bmatrix}, \qquad (2)$$

where $\varepsilon_L^{\mathbf{GG}'}$ is the atomistic longitudinal dielectric response (density-density correlation), $\varepsilon_T^{\mathbf{GG}'}$ is the atomistic transverse dielectric function (current-current correlation). The cross-coupling terms $\varepsilon_{LT}^{\mathbf{GG}'}$ and $\varepsilon_{TL}^{\mathbf{GG}'}$ represent the longitudinal and transverse dielectric responses induced by the transverse and longitudinal fields, respectively. However, in a cubic material such as Si, contributions from $\varepsilon_{TL}^{\mathbf{GG}'}$ and $\varepsilon_{LT}^{\mathbf{GG}'}$ are negligibly small [42,66], and are neglected from consideration.

In Fourier space, the induced potential $\delta V_{\text{ind}}(\mathbf{r}, t)$ in a material due to an external potential $\delta V_{\text{ext}}(\mathbf{r}, t)$ can be expressed in terms of the longitudinal dielectric function $\varepsilon_L^{\mathbf{GG}'}$ as

$$\delta V_{\text{ext}}(\mathbf{q} + \mathbf{G}, \omega) = \sum_{\mathbf{G}'} \varepsilon_L^{\mathbf{GG}'}(\mathbf{q}, \omega) \delta V_{\text{ind}}(\mathbf{q} + \mathbf{G}', \omega), \quad (3)$$

whereas $\varepsilon_T^{\mathbf{GG}'}$ is defined as

$$\frac{4\pi c}{\omega^2} \mathbf{J}_{\text{ind}}(\mathbf{q} + \mathbf{G}, \omega) = \sum_{\mathbf{G}'} [\varepsilon_T^{\mathbf{GG}'}(\mathbf{q}, \omega) - \delta_{\mathbf{GG}'}]$$
$$\cdot \mathbf{A}(\mathbf{q} + \mathbf{G}', \omega), \qquad (4)$$

where $\mathbf{J}_{\text{ind}}$ is the induced current and $\mathbf{A}$ is the transverse vector potential. We note that the transverse part of the vector potential $\mathbf{A}$ is gauge invariant.

A. Adler-Wiser longitudinal dielectric function

In the literature, the longitudinal dielectric function has been extensively studied including the local-field effects.

We neglect the exchange-correlation contribution within the relaxation time approximation [38]. Our main contribution in this section is the transverse atomistic dielectric function. However, for completeness, we restate the atomistic longitudinal dielectric function that is given by (see the Supplemental Material [67] for a detailed derivation)

$$\varepsilon_L^{\mathbf{GG'}}(\mathbf{q}, \omega) = \delta_{\mathbf{GG'}} - \frac{4\pi e^2}{q^2} \frac{1}{\Omega} \sum_{n,n',\mathbf{k}\sigma} f_{n\mathbf{k}}(1 - f_{n'\mathbf{k}+\mathbf{q}})$$

$$\times \left[\frac{\langle n, \mathbf{k}|e^{-i(\mathbf{q}+\mathbf{G})\cdot\mathbf{r}}|n', \mathbf{k}+\mathbf{q}\rangle \langle n', \mathbf{k}+\mathbf{q}|e^{i(\mathbf{q}+\mathbf{G'})\cdot\mathbf{r'}}|n, \mathbf{k}\rangle}{\epsilon_{n,\mathbf{k}} - \epsilon_{n',\mathbf{k}+\mathbf{q}} + \hbar\omega + i\hbar\alpha} + \text{c.c.} \right], \qquad (5)$$

where Ω is the crystal volume, $\mathbf{k}$ and σ are the carrier momentum and spin, $f_{n\mathbf{k}}$ is the Fermi-Dirac distribution, n, n' are the band indices, and ϵ_{nk} is the eigenenergy. Conservation of crystal momentum has been built in to the expression for the dielectric function.

This response determines the plasmon screening in a material. Also, the screened Coulomb interaction and the self-energy operator are determined by the above nonlocal longitudinal dielectric response function [57]. Hence, in GW calculations, the $\varepsilon_L^{\mathbf{GG'}}(\mathbf{q}, \omega)$ are determined including the local-field effects. In Sec. IV, we employ $\varepsilon_L^{\mathbf{GG'}}(\mathbf{q}, \omega)$ to determine the atomistic plasmon dispersion.

B. Beyond the longitudinal dielectric function: atomistic transverse dielectric response

We emphasize that the atomistic transverse dielectric function has received far less attention in the literature. The behavior of propagating electrodynamic waves (i.e., photons) is governed by the transverse response of matter. Previous work by Adler derived the transverse dielectric function by assuming both the field and induced current density as macroscopic quantities [41,68]. Here, we include all atomistic local-field contributions of the vector field and obtain the transverse dielectric function, starting from the fundamental light-matter interaction Hamiltonian

$$H = \frac{(\boldsymbol{p} - e\mathbf{A}/c)^2}{2m} + U(\mathbf{r}), \qquad (6)$$

where $U(\mathbf{r})$ is the periodic lattice potential. Both $\mathbf{J}_{\text{ind}}$ and $\mathbf{A}$ are microscopic in nature with components varying rapidly within the unit cell. Hence, the vector potential is of the form

$$\mathbf{A}(\mathbf{r'}, \omega) = \sum_{\mathbf{G'},\mathbf{q}} A_{\mathbf{G'}}(\mathbf{q}, \omega) \mathbf{t}_{\mathbf{G'}} e^{i(\mathbf{q}+\mathbf{G'})\cdot\mathbf{r'}}, \qquad (7)$$

where $\mathbf{t}_\mathbf{G}$ is the unit vector component perpendicular to $\mathbf{q} + \mathbf{G}$. In the Supplemental Material [67], we derive $\varepsilon_T^{\mathbf{GG'}}(\mathbf{q}, \omega)$. Here, we state the important contribution of our manuscript, which is

$$\varepsilon_T^{\mathbf{GG'}}(\mathbf{q}, \omega) = \delta_{\mathbf{GG'}} + \frac{4\pi e^2}{\Omega\omega^2} \sum_{n,n',\mathbf{k}} \langle n\mathbf{k}|e^{-i(\mathbf{G}+\mathbf{q})\cdot\mathbf{r}} \mathbf{t}_\mathbf{G} \cdot \mathbf{J}_0|n'\mathbf{k}+\mathbf{q}\rangle \langle n'\mathbf{k}+\mathbf{q}|e^{i(\mathbf{G'}+\mathbf{q})\cdot\mathbf{r'}} \mathbf{t}_{\mathbf{G'}} \cdot \mathbf{J}_0|n\mathbf{k}\rangle$$

$$\times (f_{n'\mathbf{k}+\mathbf{q}} - f_{n\mathbf{k}}) \left[\text{PV}\left(\frac{1}{\epsilon_{n'\mathbf{k}+\mathbf{q}} - \epsilon_{n\mathbf{k}} - \hbar\omega} \right) + i\pi\delta(\epsilon_{n'\mathbf{k}+\mathbf{q}} - \epsilon_{n\mathbf{k}} - \hbar\omega) \right], \qquad (8)$$

where $\mathbf{J}_0$ is the probability current operator and PV represents the principle value. In Sec. IV, we show that this atomistic transverse dielectric response determines the atomistic electrodynamic dispersion of a material. In Sec. V, we apply these formulae to obtain the atomistic longitudinal and transverse dielectric functions of Si based on an isotropic nearly free electron band structure.

IV. MAXWELL HAMILTONIAN IN MATTER

In this section, we develop the atomistic nonlocal electrodynamic theory of matter. We derive the Maxwell Hamiltonian in matter that depends on the spin-1 behavior of photons, analogous to the Dirac Hamiltonian for spin-1/2 particles. This formalism will be employed in the

next section to obtain the atomistic electrodynamic ω-q dispersion of a material. We emphasize that the Maxwell Hamiltonian has been used to understand the correspondence between photons and massless fermions in the Dirac equation specifically in free space. Only recently, the Maxwell Hamiltonian has regained attention in condensed matter to predict topological electrodynamic phases of matter [28]. Here we develop the Maxwell Hamiltonian formalism of matter and apply the formalism to the semiconducting material silicon.

A. Picophotonic Bloch function

Atomistic electrodynamic dispersion of matter is obtained through solutions to the Maxwell Hamiltonian corresponding to the transverse part of the electromagnetic fields. The equation of motion for the Maxwell Hamiltonian $\mathcal{H}$ (in Gaussian units) in vacuum (see Appendix A) is given by

$$\mathcal{H} \cdot \mathbf{f} = \frac{\omega}{c}\mathbf{g}, \qquad (9)$$

$$\mathbf{f} = \begin{bmatrix} \mathbf{E}_T(\mathbf{r}, \omega) \\ \mathbf{H}_T(\mathbf{r}, \omega) \end{bmatrix}, \qquad \mathbf{g} = \begin{bmatrix} \mathbf{D}_T(\mathbf{r}, \omega) \\ \mathbf{B}_T(\mathbf{r}, \omega) \end{bmatrix},$$

where

$$\mathcal{H} = \begin{bmatrix} 0 & \mathcal{H}^\dagger \\ \mathcal{H} & 0 \end{bmatrix}, \qquad \mathcal{H} = \mathbf{q} \cdot \boldsymbol{\mathcal{S}} \qquad (10)$$

with $\mathbf{q} = -i\nabla$ the momentum operator and $\boldsymbol{\mathcal{S}}$ the spin-1 operator. The Maxwell Hamiltonian is expressed in terms of spin-1 operators of the photon [69] and the components of the spin-1 operators are defined as

$$\mathcal{S}_x = \begin{bmatrix} 0 & 0 & 0 \\ 0 & 0 & -1 \\ 0 & 1 & 0 \end{bmatrix}, \qquad \mathcal{S}_y = \begin{bmatrix} 0 & 0 & 1 \\ 0 & 0 & 0 \\ -1 & 0 & 0 \end{bmatrix},$$

$$\mathcal{S}_z = \begin{bmatrix} 0 & -1 & 0 \\ 1 & 0 & 0 \\ 0 & 0 & 0 \end{bmatrix}, \qquad (11)$$

and they satisfy the angular momentum algebra $[\mathcal{S}_i, \mathcal{S}_j] = \epsilon_{ijk}\mathcal{S}_k$. Given a translation operator $\mathcal{T}$, the field vector $\mathbf{f}(\mathbf{r}, \omega)$ and the displacement vector $\mathbf{g}(\mathbf{r}, \omega)$ follow the relations

$$\mathcal{T} \cdot \mathbf{f}(\mathbf{r}, \omega) = \mathbf{f}(\mathbf{r} + \mathbf{R}, \omega),$$
$$\mathcal{T} \cdot \mathbf{g}(\mathbf{r}, \omega) = \mathbf{g}(\mathbf{r} + \mathbf{R}, \omega). \qquad (12)$$

It is easy to see that the Maxwell Hamiltonian commutes with the translation operator, $[\mathcal{T}, \mathcal{H}] = 0$. In vacuum, the eigenfields to the Maxwell Hamiltonian will be simple plane waves $\mathbf{f} \sim e^{i\mathbf{q}\cdot\mathbf{r}}$. However, inside a material, the Maxwell Hamiltonian is modulated by a periodic dielectric

response; hence, the eigenfields will take the Bloch form [70]

$$\mathbf{f_q}(\mathbf{r}, \omega) = e^{i\mathbf{q}\cdot\mathbf{r}}\mathbf{u_q}(\mathbf{r}, \omega), \qquad (13)$$

where $\mathbf{u_q}$ is the picophotonic Bloch function, a periodic vector function with the same periodicity as the crystal, and $\mathbf{q}$ is the photon momentum. The picophotonic Bloch function $\mathbf{u_q}$ can be expanded as a Fourier series of plane waves $e^{i\mathbf{G}\cdot\mathbf{r}}$, with $\mathbf{G}$ being the reciprocal lattice vector

$$\mathbf{u_q}(\mathbf{r}, \omega) = \sum_{\mathbf{G}} \boldsymbol{\mathcal{U}}_{\mathbf{G}}(\mathbf{q}, \omega)e^{i\mathbf{G}\cdot\mathbf{r}}, \qquad (14)$$

where $\boldsymbol{\mathcal{U}}_{\mathbf{G}} = [\mathbf{E_G}, \mathbf{H_G}]^T$.

B. Picophotonic eigenvalue equation

In a material, the response to an external probe is captured by the displacement field $\mathbf{g_q}(\mathbf{r}, \omega) = \sum_{\mathbf{G}}\boldsymbol{\mathcal{V}}_{\mathbf{G}}(\mathbf{q}, \omega)e^{i\mathbf{G}\cdot\mathbf{r}}$ with $\boldsymbol{\mathcal{V}}_{\mathbf{G}} = [\mathbf{D_G}, \mathbf{B_G}]^T$. Within a linear response framework, the atomistic displacement field $\boldsymbol{\mathcal{V}}_{\mathbf{G}}$ can be expressed as

$$\boldsymbol{\mathcal{V}}_{\mathbf{G}} = \sum_{\mathbf{G}'} \boldsymbol{\mathcal{R}}_{\mathbf{GG}'} \cdot \boldsymbol{\mathcal{U}}_{\mathbf{G}'},$$

$$\begin{bmatrix} \mathbf{D_G} \\ \mathbf{B_G} \end{bmatrix} = \sum_{\mathbf{G}'} \begin{bmatrix} \varepsilon_T^{\mathbf{GG}'}(\mathbf{q}, \omega) & \xi_T^{\mathbf{GG}'}(\mathbf{q}, \omega) \\ \tau_T^{\mathbf{GG}'}(\mathbf{q}, \omega) & \mu_T^{\mathbf{GG}'}(\mathbf{q}, \omega) \end{bmatrix} \cdot \begin{bmatrix} \mathbf{E_{G'}} \\ \mathbf{H_{G'}} \end{bmatrix},$$

where $\boldsymbol{\mathcal{R}}_{\mathbf{GG}'}$ is the generalized linear response matrix, which includes permittivity ε, permeability μ, and magnetoelectric coupling τ, ξ. The component $\boldsymbol{\mathcal{R}}_{\mathbf{GG}'}(\mathbf{q}, \omega)$ can be thought of as the linear response observed in a given material at a field point $\mathbf{q} + \mathbf{G}'$ (in reciprocal lattice space) due to a perturbation at the source point $\mathbf{q} + \mathbf{G}$. This form can now be substituted into Eq. (9), and the picophotonic eigenvalue equation is given by

$$\mathcal{H}(\mathbf{q} + \mathbf{G}) \cdot \begin{bmatrix} \mathbf{E_G} \\ \mathbf{H_G} \end{bmatrix} = \frac{\omega}{c} \sum_{\mathbf{G}'} \boldsymbol{\mathcal{R}}_{\mathbf{GG}'}(\mathbf{q}, \omega) \cdot \begin{bmatrix} \mathbf{E_{G'}} \\ \mathbf{H_{G'}} \end{bmatrix}. \qquad (15)$$

Matrix $\boldsymbol{\mathcal{R}}_{\mathbf{GG}'}$ should build in the space group symmetry of the Brillouin zone, and $\mathbf{G}, \mathbf{G}' \neq 0$ terms in the matrix encode the inhomogeneity due to the microscopic response of the electrons (the local fields). The above Hamiltonian equation depends nonlinearly on the eigenvalue ω due to functional ω dependency of the response matrix $\boldsymbol{\mathcal{R}}_{\mathbf{GG}'}(\mathbf{q}, \omega)$. Such a class of equations is known as the nonlinear eigenvalue problem. Solutions to this generalized nonlinear eigenvalue problem results in the atomistic electrodynamic dispersion of a material that represents transverse photon interaction in a material system.

We note that the above Maxwell Hamiltonian equation of motion is based on the plane-wave expansion, whose

solutions result in the atomistic electrodynamic dispersion. Similarly, it is well known that the electronic band structure of a material can be determined by the plane-wave expansion of the Schrödinger Hamiltonian of the form [71]

$$\sum_{\mathbf{G}'} \left[\frac{\hbar^2 |\mathbf{q} + \mathbf{G}|^2}{2m} \delta_{\mathbf{GG}'} + V(\mathbf{G} - \mathbf{G}') \right] U(\mathbf{G}') = EU(\mathbf{G}), \tag{16}$$

and the corresponding electronic wave function will be of the form $\psi(\mathbf{r}) = e^{i\mathbf{k} \cdot \mathbf{r}} \sum_{\mathbf{G}} U(\mathbf{G}) e^{i\mathbf{G} \cdot \mathbf{r}}$. Hence, the burden of determining the electronic band structure of a material falls upon the accurate determination of the pseudopotential coefficients $V(\mathbf{G} - \mathbf{G}')$. In a similar manner, one needs to obtain the response matrix $\mathcal{R}_{\mathbf{GG}'}(\mathbf{q}, \omega)$ to deduce the atomistic electrodynamic dispersion. In Si, only the atomistic dielectric function $\varepsilon_T^{\mathbf{GG}'}$ has considerable contributions, $\mu_T = 1$ and $\xi_T = \tau_T = 0$. In Sec. V, $\varepsilon_T^{\mathbf{GG}'}(\mathbf{q}, \omega)$ and the atomistic electrodynamic dispersion of Si are obtained within an isotropic nearly free electron model.

C. Picoplasmonic dispersion

Here, we go beyond the well-known definitions of nanoscale plasmons and epsilon-near-zero materials that use the macroscopic response of matter. We show that the atomistic electrodynamic theory reveals a dispersion relation that embodies the symmetries of the underlying lattice. A plasmon is a self-sustained charge oscillation induced by a longitudinal electric field without the introduction of external charge densities. Since the longitudinal field is purely determined by the scalar potential, from Eq. (3), we see that the condition for sustained plasma excitation in a material is given by

$$\det[\varepsilon_L^{\mathbf{GG}'}(\mathbf{q}, \omega)] = 0. \tag{17}$$

Using the above relation, we can obtain the eigenfrequencies ω for a fixed $\mathbf{q}$. Hence, solving this equation one can obtain the atomistic plasmon dispersion of the material. In the continuum limit, we obtain the standard relation

$$\varepsilon_M(\mathbf{q}, \omega) = 0, \tag{18}$$

where the macroscopic dielectric function ε_M is defined as

$$\varepsilon_M(\omega) = \lim_{\mathbf{q} \to 0} \frac{1}{(\varepsilon_L^{\mathbf{GG}'})_{00}^{-1}}, \tag{19}$$

where $(\varepsilon_L^{\mathbf{GG}'})_{00}^{-1}$ is the first diagonal component of the inverse longitudinal dielectric matrix. Inverse operation indirectly includes the off-diagonal local-field effect contributions. Alternatively, in the literature, the plasmon

dispersion is determined by identifying the peaks of the energy-loss function

$$L(\mathbf{q}, \omega) = -\operatorname{Im} \varepsilon_M^{-1}(\mathbf{q}, \omega),$$

$$= \frac{\varepsilon_2(\mathbf{q}, \omega)}{[\varepsilon_1(\mathbf{q}, \omega)]^2 + [\varepsilon_2(\mathbf{q}, \omega)]^2}, \tag{20}$$

where we have taken $\varepsilon_M = \varepsilon_1 + i\varepsilon_2$. This is known as the experimental definition of the plasmon dispersion [12]. At the plasmon frequency ω_p, $\varepsilon_1(\mathbf{q}, \omega_p) \approx 0$ and the damping factor ε_2 is small, so that we observe peaks in the energy-loss spectrum [72,73]. However, we note that Eq. (17) provides the most general theoretical relation to obtain the atomistic plasmon dispersion of a material [74].

V. APPLICATION TO SILICON

Silicon has the diamond cubic crystal structure [Fig. 2(a)] and the first Brillouin zone has the shape of a truncated octahedron [Fig. 2(b)]. It has been shown earlier [75,76] that the momentum-dependent dielectric function in diamond-type materials is insensitive to the direction of $\mathbf{q}$. Hence, we can replace the truncated octahedron shape [Fig. 2(b)] of the first Brilloin zone by a sphere [Fig. 2(d)] and obtain the dielectric properties through an isotropic model. Moreover, dielectric screening is not sensitive to the details of the band structure since it involves all the valence electrons in the material [77]. We show that the results obtained through an isotropic nearly free electron band structure agrees well with the exact band-structure models for Si.

The nearly free electron model employed here was first introduced by Penn [77,78]. This model allows for the formation of standing waves at the Brillouin zone boundaries and accounts for the Umklapp processes [79]. In this scheme, the eigenenergy and wave functions of an electron are given by

$$E_{\mathbf{k}}^{\pm} = \frac{1}{2} \left[E_{\mathbf{k}}^0 + E_{\mathbf{k}'}^0 \pm \sqrt{(E_{\mathbf{k}}^0 - E_{\mathbf{k}'}^0)^2 + E_g^2} \right],$$

$$\psi_{\mathbf{k}}^{\pm} = \frac{e^{i\mathbf{k} \cdot \mathbf{r}} + \alpha_{\mathbf{k}}^{\pm} e^{i\mathbf{k}' \cdot \mathbf{r}}}{\sqrt{1 + (\alpha_{\mathbf{k}}^{\pm})^2}}, \tag{21}$$

where

$$\alpha_{\mathbf{k}}^{\pm} = \frac{E_g}{2(E_{\mathbf{k}}^{\pm} - E_{\mathbf{k}'}^0)}, \qquad E_{\mathbf{k}}^0 = \frac{\hbar^2 k^2}{2m}, \qquad \mathbf{k}' = \mathbf{k} - \mathbf{G}_1,$$

$\mathbf{G}_1 = 2k_f \hat{k}$, k_f is the valence Fermi wave vector, and E_g is the band gap of the material. Superscripts "+" and "−" represent $k > k_f$ (conduction) and $k < k_f$ (valence) bands, respectively. The experimentally measured valence electron density for Si is $n_0 = 0.19 \ e^-/\text{Å}^3$. Now consider a free-electron solid with the same density. This will form a
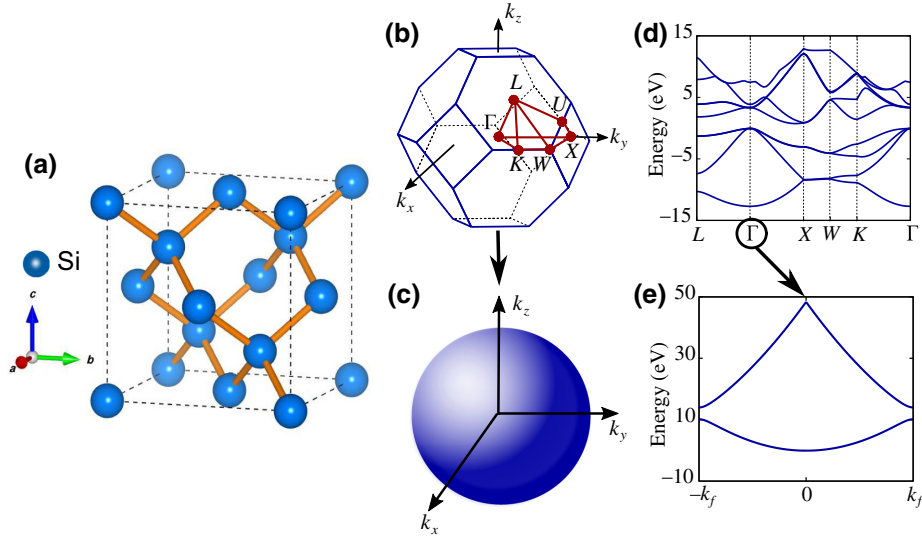
FIG. 2. (a) Cubic crystal structure of silicon is shown. (b) First Brillouin zone of silicon, a truncated octahedron is plotted in k space. (c) Spherical Brillouin zone used in this work to obtain the dielectric properties is plotted in k space. (d) Band structure of silicon obtained using the empirical pseudopotential method. (e) Band structure of silicon within a nearly free electron model. This isotropic model can be thought of as a symmetric expansion of the band structure around the high-symmetric Γ point.

Fermi sphere in momentum space. According to Sommerfeld theory [80], the corresponding valence Fermi wave vector in Si is $k_f = (3\pi^2 n_0)^{1/3} = 1.78$ Å^{-1}. This will form the fully occupied valence band. An additional conduction band with band gap E_g is constructed to reflect the semiconducting nature of Si. Wave function components with wave vector $\mathbf{k}' = \mathbf{k} - \mathbf{G}_1$ facilitate the Umklapp process. For a given photon momentum $\mathbf{q}$, $\mathbf{k} \rightarrow \mathbf{k} + \mathbf{q}$ indicates the normal process and $\mathbf{k} \rightarrow \mathbf{k} + \mathbf{q} + \mathbf{G}_1$ is the Umklapp process.

In Figs. 2(c) and 2(e), we respectively plot the exact band structure and the isotropic nearly free electron band structure of Si considered here. The nearly free electron band structure can be thought of as an isotropic symmetric expansion of the electronic band structure around the high-symmetric Γ point. This model can reproduce the experimentally observed dielectric properties [81] of silicon (See Fig. S1 within the Supplemental Material [67]).

We now proceed to obtain the atomistic longitudinal and transverse dielectric functions of Si using this model. Through inspection, we see that, for either case, within this model only the dielectric matrix elements corresponding to $\mathbf{G} = 0$ and $\mathbf{G}_1 = 2k_f \hat{k}$ are nonzero. All higher-order elements corresponding to the reciprocal lattice vectors vanish.

Typically, the dielectric function of a material is considered to be only a function of ω. In Fig. 3, we observe a family of curves dependent on the wave vector q even at a fixed ω. Moreover, the evolution of longitudinal and transverse dielectric functions are found to be inequivalent at $\mathbf{q} \neq 0$. We note that $\varepsilon_L^{ij}(q \neq 0, \omega)$ and

$\varepsilon_T^{ij}(q \neq 0, \omega)$ represent the atomistic nonlocal contributions to the dielectric properties. Functions ε_L^{01}, ε_T^{01} (corresponding to $\mathbf{G} = 0, \mathbf{G}' = \mathbf{G}_1$) and ε_L^{11}, ε_T^{11} (corresponding to $\mathbf{G} = \mathbf{G}' = \mathbf{G}_1$) are due to the local-field effects. Functions $\varepsilon_L^{00}(q \neq 0, \omega)$ and $\varepsilon_T^{00}(q \neq 0, \omega)$ determine the dielectric response of a material at a source and field point on the sphere of radius q. Since we have considered an isotropic electron model, this dielectric response is identical at all points on this sphere, whereas $\varepsilon_{L,T}^{01}(q \neq 0, \omega)$ determines the material response at a field point $\mathbf{q} + \mathbf{G}_1$ from a source point $\mathbf{q}$ in momentum space, and $\varepsilon_{L,T}^{11}(q \neq 0, \omega)$ is the dielectric response from a source and field point, both at $\mathbf{q} + \mathbf{G}_1$. These scenarios are pictorially depicted in Fig. 3.

In the literature, typically only the longitudinal dielectric function in the long-wavelength limit $\varepsilon_L^{00}(\mathbf{q} = 0, \omega)$ is calculated and used to obtain all dielectric properties of the material. Our calculations show that at finite momentum ($\mathbf{q} \neq 0$), transverse and longitudinal dielectric functions are inequivalent, and the higher-order components have significant contributions to the dielectric properties even at $\omega = 0$. In our analysis we neglect the damping factor contributions in the dielectric response. In the next section, we show that the local-field contributions lead to an additional anomalous band formation in the atomistic electrodynamic dispersion of Si.

VI. ANOMALOUS BAND IN THE FORBIDDEN GAP

In this section, we apply the Maxwell Hamiltonian theory of matter described in Sec. IV to obtain the atomistic electrodynamic ω-q dispersion in Si. We show the
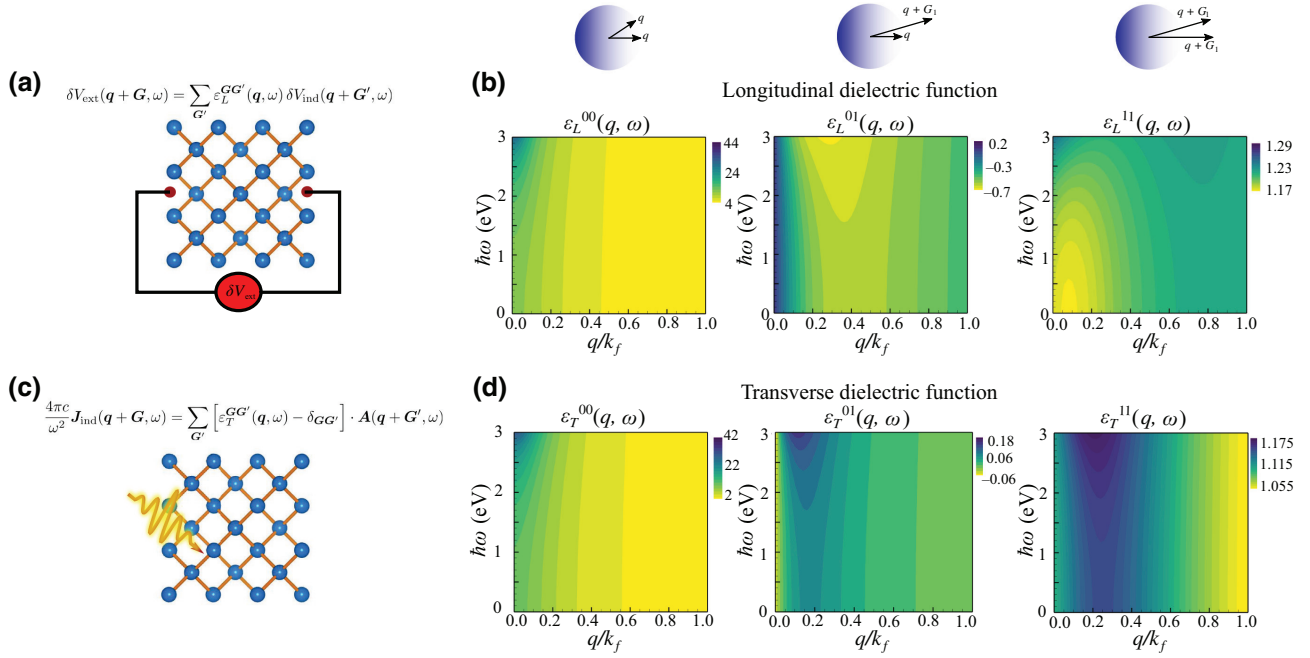
FIG. 3. (a) Within the linear response theory, induced potential $\delta V_{\text{ind}}(r, t)$ in a material due to an external potential $\delta V_{\text{ext}}(r, t)$ can be expressed in terms of the longitudinal dielectric function $\varepsilon_L^{\mathbf{GG'}}$. (c) The atomistic transverse dielectric function $\varepsilon_T^{\mathbf{GG'}}$ determines the linear response of a material to a transverse electromagnetic pulse. Contour plots of the atomistic (b) longitudinal and (d) transverse dielectric function components for silicon are displayed as a function of frequency ω and wave vector q.

existence of anomalous atomistic waves in the band gap of silicon. We also directly compare with existing theories to recover well-known waves and also prove that the anomalous waves are the result of atomistic electrodynamics.

Components of the atomistic transverse dielectric function are obtained through the isotropic nearly free-electron model [see Fig. 3(b)]. We compare macroscopic electrodynamic approaches to atomistic nonlocal electrodynamic theory in the sections below.

A. Macroscopic local theory

In a macroscopic local electrodynamic theory, the dielectric function is only dependent on the frequency while the local-field effects are ignored. Hence, only $\varepsilon_T^{00}(q = 0, \omega)$ contributes to the dielectric properties of the material. For a given frequency, ε_T^{00} is considered constant across the momentum range [Fig. 4(a)]. In a macroscopic theory, transverse electromagnetic waves satisfy the continuum relation

$$q^2 = \varepsilon_T^{00}(q = 0, \omega) \frac{\omega^2}{c^2}. \tag{22}$$

The solution to the above equation results in the electrodynamic dispersion shown in Fig. 5(a). We observe the light line behavior retained for small-q values. A band gap is observed in the spectrum, corresponding to the region $\varepsilon_T^{00} < 0$. At large-q values photons are localized

(zero slope of the band) consistent with the local dielectric response considered here.

B. Macroscopic nonlocal theory

The dielectric function behavior at $q \neq 0$ determines the nonlocal response of the material. Hence, in the case of a macroscopic nonlocal theory, we consider the dielectric response to be $\varepsilon_T^{00}(q, \omega)$ and the local-field effects are again
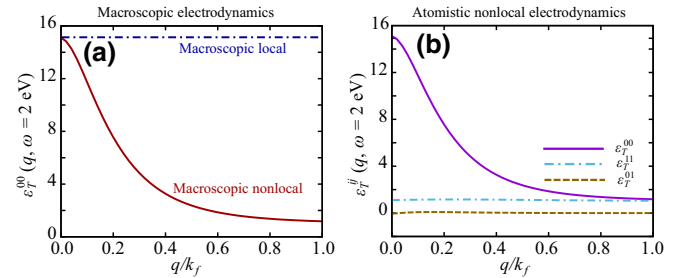

FIG. 4. The atomistic transverse dielectric function $\varepsilon_T^{ij}(q, \hbar\omega = 2 \text{ eV})$ is plotted as a function of wave vector q. (a) In a macroscopic local theory, the dielectric component ε_T^{00} is independent of q, whereas in the case of the macroscopic nonlocal framework, only the $\varepsilon_T^{00}(q, \omega)$ component is considered, and the local-field effects are neglected. (b) In an atomistic nonlocal theory, $\varepsilon_T^{00}, \varepsilon_T^{01}$, and ε_T^{11} components have significant variation with q and contribute to the overall dielectric response of the material.
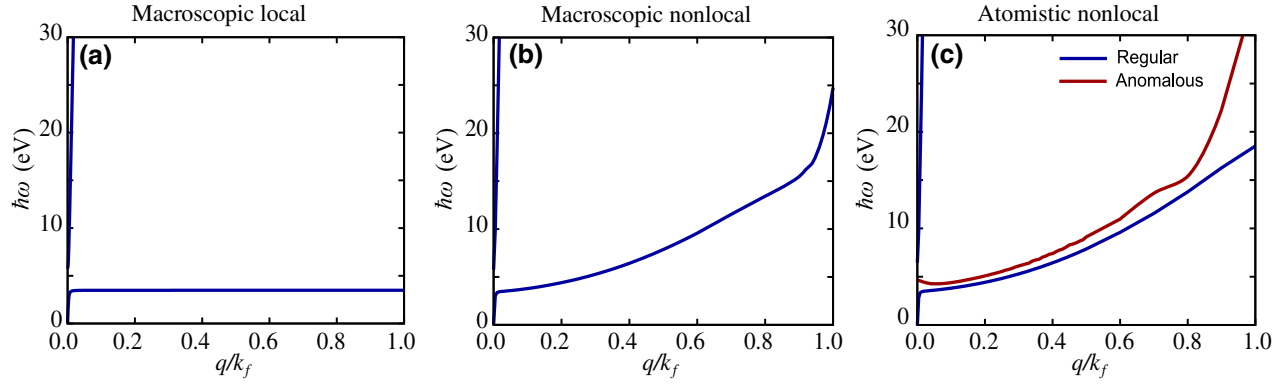
FIG. 5.   Atomistic electrodynamic dispersion of silicon is plotted as a function of momentum obtained through (a) a macroscopic local electromagnetic theory, (b) a macroscopic nonlocal theory, and (c) an atomistic nonlocal electrodynamic theory. In complete contrast to the macroscopic calculations, in the latter case of picophotonics, we observe the emergence of an anomalous band in the atomistic electrodynamic dispersion.

neglected. In Fig. 4(a), we compare the dielectric function behavior considered within a macroscopic local theory and a macroscopic nonlocal theory. With an increase in momentum, we observe a decaying behavior in the dielectric function $\varepsilon_T^{00}(q, \omega)$ at any given frequency. Within this framework, transverse electromagnetic waves satisfy the continuum relation

$$q^2 = \varepsilon_T^{00}(q, \omega) \frac{\omega^2}{c^2}. \qquad (23)$$

In Fig. 5(b), we observe that at large-q values, electrodynamic bands have a finite slope due to the nonlocal response of the material. We call the dispersion curves observed in Figs. 5(a) and 5(b) through a macroscopic theory regular bands.

C. Atomistic nonlocal electrodynamic theory

In Fig. 4, we compare the dielectric response in a macroscopic theory and an atomistic electrodynamic theory. In a macroscopic theory, local-field effects are neglected. Hence, the dielectric response has a single component. However, we see that the higher-order dielectric components $\varepsilon_T^{01}, \varepsilon_T^{11}$ have small but non-negligible contributions to the overall dielectric response of the material. The generalized nonlinear picophotonic eigenvalue problem in Eq. (15) is solved to obtain the atomistic electrodynamic dispersion (see the Supplemental Material [67] for the solution to the nonlinear picophotonic eigenvalue problem).

In Fig. 5(c) we see that, along with regular bands, an anomalous band is also observed in the dispersion. This anomalous band is absent if we treat the problem using macroscopic local or macroscopic nonlocal electrodynamic frameworks. Hence, the anomalous band is a direct consequence of the inclusion of local-field effects

in Si. Even at $q = 0$, the anomalous band has a finite frequency. This is in stark contrast with the regular band, whose frequency vanishes at $q = 0$. In classical optical theories one would consider this regime to be perfectly metallic where the propagation of light is forbidden. However, from Fig. 5(c), we see that the light can propagate through silicon in the picophotonics regime.

In Fig. 6, we plot the normalized electromagnetic field at $q = 0.178$ nm^{-1} in Si hosted by the regular and anomalous bands. Across the momentum, the regular band has wavelengths in nanometers, whereas the anomalous band has
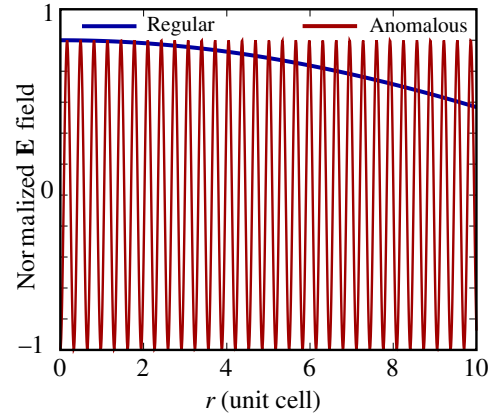

FIG. 6.   Normalized electric field is plotted at $q = 0.178$ nm^{-1} for the regular and anomalous bands. Here, the regular band (blue curve) has wavelength $\lambda = 35.30$ nm. In contrast, the anomalous band (red curve) has wavelength $\lambda = 0.18$ nm in the picophotonics regime. Field equations here follow the picophotonic Bloch form $\mathbf{E}_q = e^{-i\omega t} e^{iqr}(E_0 + E_1 e^{i2k_f r}) \hat{q}_\perp$. The E_0 component predominates over the E_1 component for the regular band, and vice versa for the anomalous band. Hence, we observe a substantial disparity between the wavelengths of the regular and anomalous bands.
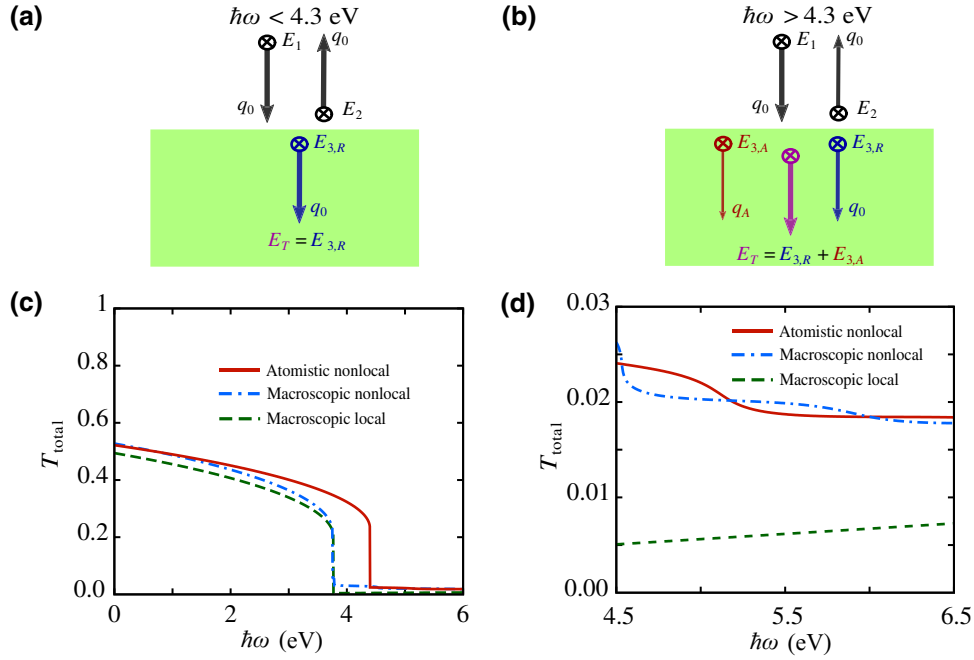
FIG. 7. Proposed experiment for verification of atomistic effects. (a) For energies $\hbar\omega < 4.3$ eV, only the regular band contributes to the total transmission in a silicon block. (b) For energies $\hbar\omega > 4.3$ eV, both regular and anomalous bands are excited by an electromagnetic wave incident on a silicon block. (c) The total transmission coefficient T_{total} at normal incidence is plotted as a function of energy $\hbar\omega$. (d) The total transmission coefficient at normal incidence is plotted as a function of energy in the deep ultraviolet regime, where both regular and anomalous bands contribute to the total transmission. We observe a clear difference in the behavior of T_{total} obtained using the atomistic nonlocal theory compared to the macroscopic theory. This difference is attributed to the contributions from the anomalous band.

subnanometer wavelengths. The lattice constant of a silicon unit cell is 0.543 nm; hence, electromagnetic waves in the anomalous band are found to be highly oscillatory within a unit cell, leading into the picophotonics regime.

For completeness, in Appendix B, we calculate the atomistic plasmon dispersion of Si obtained within the isotropic nearly free electron model. In Fig. 8 in Appendix B, we observe that the atomistic nonlocal theory and macroscopic nonlocal theory result in a nearly identical plasmon dispersions across the momentum range.

D. Experimental probe of anomalous atomistic waves

We propose an experiment to probe the atomistic picophotonic dispersion relation in silicon. Consider an electromagnetic wave incident normally on an Si block [see Fig. 7(a)]. Experimentally, one can control the energy, whereas the momentum within the crystal is determined by the atomistic electrodynamic dispersion. We calculate the transmission coefficient at two different energy ranges: (a) $\hbar\omega < 4.3$ eV and (b) $\hbar\omega > 4.3$ eV. For energies $\hbar\omega < 4.3$ eV, only the regular band is excited. Hence, the total transmission in the Si block will have contributions only from the regular band [Fig. 7(a)]. From Fig. 5(c) we see that, for energies $\hbar\omega > 4.3$ eV, both regular and anomalous bands are excited with two distinct

momentums. Hence, the total transmission should include additional terms from the interference effects due to field contributions of the anomalous band (see the Supplemental Material [67] for the derivation of total transmission).

In Fig. 7(c), we plot the total transmission coefficient calculated using the macroscopic local theory, macroscopic nonlocal theory, and the atomistic nonlocal theory. We observe that all three calculations have similar results for low energies. However, in the deep ultraviolet regime (DUV) ($\hbar\omega > 4.3$ eV), as shown in Fig. 7(d), the behavior of atomistic nonlocal theory differs from that of macroscopic local theory and macroscopic nonlocal theory. We note that in the DUV regime, the anomalous band generates additional electromagnetic energies at a given frequency of light. This additional energy contribution is reflected in the behavior of the total transmission coefficient determined through our atomistic nonlocal theory.

Experimentally, one can measure the total transmission in the range 4.5 eV $< \hbar\omega <$ 6.5 eV by shining an ultraviolet light on a silicon block. The total transmission can be accurately measured using high sensitivity single-photon detectors. The difference in the measured total transmission coefficient to that of macroscopic electrodynamic calculations should reveal the existence of anomalous bands in the atomistic electrodynamic dispersion. In our

calculations we have not considered the phonon-mediated interband transitions in silicon. Based on the experimental data [82] that is currently available from the literature, we believe that the linear regime predominates for optical intensity below 0.02 J/cm^2. Hence, we predict to observe anomalous waves in this low-intensity regime. Also, experiments [83] have shown that below 5.5 K, two-photon processes in silicon are significantly reduced by 50%. Hence, the low-temperature experiments are well suited to studying the linear regime discussed in this article.

VII. CONCLUSIONS

We develop the atomistic nonlocal electrodynamic theory of matter through a Maxwell Hamiltonian framework. We introduce the atomistic transverse dielectric tensor that determines the linear response of a material to a transverse electromagnetic probe. The electrodynamics of matter is considered within the Maxwell Hamiltonian framework, which captures the spin-1 nature of photons. Through this formulation, we discover anomalous waves in the atomistic electrodynamic dispersion of silicon. Local-field effects included in the Maxwell Hamiltonian are essential to obtain the anomalous waves in the atomistic electrodynamic dispersion. These waves are highly oscillatory within a unit cell and have subnanometer wavelengths in the picophotonics regime. The anomalous wave generates an additional electromagnetic energy contribution that was previously unaccounted for. Experimental signatures for this additional electromagnetic energy contribution can be deduced from the total transmission coefficient in the deep ultraviolet regime. We note that the frequencies corresponding to the anomalous waves are forbidden in a macroscopic local model, and are a signature of our quantum theory of atomic polarization developed here.

Our findings demonstrate that natural media can itself host several interesting electrodynamic phases. As such, the electrodynamic phases we discuss here are properties of atomistic matter itself and are not related to some form of macroscopic engineering. In this study we consider Si as a prototype material. Ge, AlSb, ZnSe, GaAs, GaP, InP, ZnS, ZnTe, CdTe are all expected to display the anomalous band, since all these material systems have the same crystal symmetry as Si.

A variety of focused electron- and ion-based techniques have recently shown compelling ways to manufacture atomic structures with atomic precision in solids [84]. Currently available electron microscopes can manipulate atomic structures, visualize them with picometer-level accuracy, and infer their electronic and photonic properties [85]. Recently, it has been demonstrated that using atomic force microscopes one can embed atom by atom in a silicon wafer to achieve single-atom control [86]. Moreover, the enhancement of local-field effects is the key to inherit

anomalous waves in the atomistic electrodynamic dispersion of materials. Materials such as MnBi [87], SiO$_4$, and selenium [68] have long been known to possess significantly enhanced local-field effects. Magneto-optical effects in MnBi are one of the manifestations of local-field effects, which can be substantially enhanced through systematic doping of Al ions to form MnBi$_x$Al$_{1-x}$ [87]. Hence, we believe that engineering the picophotonic media is well within the current capabilities of material science and engineering.

Furthermore, results presented here bring forth the importance of the atomistic electrodynamic phases of matter, and the immediate need to develop first-principles-based atomistic nonlocal electrodynamics of matter to obtain the atomistic electrodynamic dispersion of natural materials. We envision the development of picophotonic electrodynamic density functional theory for photons hosted by matter to reveal effects connected to the atomistic electrodynamic dispersion. Our analysis provides the fist step towards the discovery of topological electrodynamic properties in natural materials.

APPENDIX A: MAXWELL HAMILTONIAN IN FREE SPACE

In this appendix, we derive the Maxwell Hamiltonian discussed in Sec. IV. Maxwell's equations (in Gaussian units) are given by

$$\nabla \cdot \mathbf{E} = 4\pi\rho, \qquad \nabla \cdot \mathbf{B} = 0,$$

$$\nabla \times \mathbf{E} = -\frac{1}{c}\frac{\partial \mathbf{B}}{\partial t}, \qquad \nabla \times \mathbf{B} = \frac{1}{c}\frac{\partial \mathbf{E}}{\partial t} + \frac{4\pi}{c}\mathbf{J}. \quad \text{(A1)}$$

Along with the above equations, the charge density and current density have to satisfy the continuity equation

$$\nabla \cdot \mathbf{J} + \frac{\partial \rho}{\partial t} = 0. \quad \text{(A2)}$$

Fields can be expressed in terms of the scalar and vector potentials of the form

$$\mathbf{E} = -\nabla V - \frac{1}{c}\frac{\partial \mathbf{A}}{\partial t}, \qquad \mathbf{B} = \nabla \times \mathbf{A}. \quad \text{(A3)}$$

These potentials satisfy the gauge transformations

$$V \to V - \frac{1}{c}\frac{\partial \Xi}{\partial t}, \qquad \mathbf{A} \to \mathbf{A} + \nabla \Xi, \quad \text{(A4)}$$

where Ξ is the gauge function. It is convenient to decompose the electric field in terms of longitudinal and transverse components, given by

$$\mathbf{E}(\mathbf{r},t) = \mathbf{E}_L(\mathbf{r},t) + \mathbf{E}_T(\mathbf{r},t), \tag{A5}$$

where $\nabla \cdot \mathbf{E}_T(\mathbf{r},t) = 0$ and $\nabla \times \mathbf{E}_L(\mathbf{r},t) = 0$. Note that the magnetic field will only have a transverse component due to the zero-divergence condition. With this decomposition, one can write

$$\nabla \cdot \mathbf{E}_L = 4\pi\rho, \qquad \nabla \cdot \mathbf{B}_T = 0,$$
$$\nabla \times \mathbf{E}_T = -\frac{1}{c}\frac{\partial \mathbf{B}_T}{\partial t}, \qquad \nabla \times \mathbf{B}_T = \frac{1}{c}\frac{\partial \mathbf{E}}{\partial t} + \frac{4\pi}{c}\mathbf{J}, \tag{A6}$$

and the corresponding gauge transformations are given by

$$V \to V - \frac{1}{c}\frac{\partial \Xi}{\partial t}, \quad \mathbf{A}_L \to \mathbf{A}_L + \nabla\Xi, \quad \mathbf{A}_T \to \mathbf{A}_T. \tag{A7}$$

We can choose the gauge function Ξ such that $\mathbf{A}_L = 0$. Hence,

$$\mathbf{E}_L = -\nabla V, \quad \mathbf{E}_T = -\frac{1}{c}\frac{\partial \mathbf{A}_T}{\partial t}, \quad \mathbf{B} = \nabla \times \mathbf{A}_T. \tag{A8}$$

Hence, the longitudinal electric field $\mathbf{E}_L$ is purely determined by the scalar potential. The Maxwell Hamiltonian is related to the transverse part of the electromagnetic fields. We first consider the Ampére-Maxwell equation given by

$$\nabla \times \mathbf{B}_T = \frac{1}{c}\frac{\partial \mathbf{E}}{\partial t} + \frac{4\pi}{c}\mathbf{J},$$
$$= \frac{1}{c}\frac{\partial \mathbf{E}_L}{\partial t} + \frac{1}{c}\frac{\partial \mathbf{E}_T}{\partial t} + \frac{4\pi}{c}\mathbf{J}_L + \frac{4\pi}{c}\mathbf{J}_T. \tag{A9}$$

We can show that

$$\nabla \cdot \frac{\partial \mathbf{E}_L}{\partial t} = 4\pi\frac{\partial \rho}{\partial t}, = -4\pi\nabla \cdot \mathbf{J}_L.$$

Hence,

$$\frac{\partial \mathbf{E}_L}{\partial t} = -4\pi\mathbf{J}_L. \tag{A10}$$

Using this relation, we can simplify Eq. (A9) as

$$\nabla \times \mathbf{B}_T = \frac{1}{c}\frac{\partial \mathbf{E}_T}{\partial t} + \frac{4\pi}{c}\mathbf{J}_T. \tag{A11}$$

We are interested in the response of a bulk material. Therefore, it is convenient to represent the induced charges and

current in terms of the polarization $\mathbf{P}$ and magnetization density $\mathbf{M}$,

$$\rho = -\nabla \cdot \mathbf{P}_L, \qquad \mathbf{J} = \frac{\partial \mathbf{P}}{\partial t} + c\,\nabla \times \mathbf{M}. \tag{A12}$$

The equations of motion in terms of the displacement fields $\mathbf{D} = \mathbf{E} + 4\pi\mathbf{P}$ and $\mathbf{H} = \mathbf{B} - 4\pi\mathbf{M}$ are given by

$$\nabla \times \mathbf{E}_T = -\frac{1}{c}\frac{\partial \mathbf{B}_T}{\partial t}, \qquad \nabla \times \mathbf{H}_T = \frac{1}{c}\frac{\partial \mathbf{D}_T}{\partial t}. \tag{A13}$$

Hamiltonian form presented in Eq. (9) immediately follows if we define $\mathbf{f} = [\mathbf{E}_T, \mathbf{H}_T]^T$ and $\mathbf{g} = [\mathbf{D}_T, \mathbf{B}_T]^T$.

APPENDIX B: ATOMISTIC PLASMON DISPERSION IN SILICON

The atomistic plasmon dispersion of Si has previously been studied in literature both theoretically [12] and experimentally [88]. For completeness, in this appendix, we present the atomistic plasmon dispersion obtained using the isotropic nearly free electron model. In Fig. 3(b), we display $\varepsilon_L^{00}(q,\omega)$, $\varepsilon_L^{01}(q,\omega)$, and $\varepsilon_L^{11}(q,\omega)$ for Si obtained using this model. We can substitute these functions into Eq. (17) to obtain the plasmon dispersion using the atomistic nonlocal electrodynamic theory (Fig. 8). As earlier, we compare the dispersion obtained through the macroscopic local theory and macroscopic nonlocal theory.

In the case of macroscopic local theory, the dielectric function $\varepsilon_L^{00}(q = 0, \omega)$ is considered independent of $\mathbf{q}$. Hence, the plasmon dispersion curve is observed to be a straight line with zero slope and intercept given by the zero of $\varepsilon_L^{00}(q = 0, \omega)$. In the macroscopic nonlocal
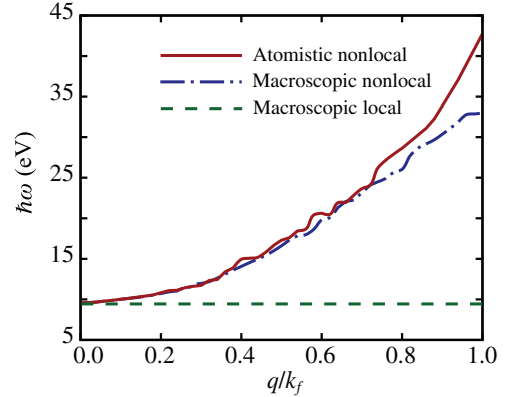

FIG. 8. Atomistic plasmon dispersion of silicon is plotted as a function of wave vector q. We compare the results obtained through a macroscopic local theory, macroscopic nonlocal theory, and an atomistic nonlocal electrodynamic theory. Macroscopic nonlocal and atomistic nonlocal electrodynamic theory results in nearly identical plasmon dispersion. However, we note that the picophotonic effects are fundamentally different, as emphasized in the main text.

theory, plasmon frequencies are determined by the condition $\varepsilon_L^{00}(q, \omega) = 0$. Both macroscopic nonlocal theory and atomistic nonlocal theory results in nearly identical plasmon dispersion, diverging slightly only at very large q. We note that at $q = 0$, plasmon frequency (about 9.6 eV) obtained through the isotropic nearly free electron model slightly underestimates the corresponding experimentally observe value (about 16 eV) [88].

---

[1] Marvin L. Cohen and Steven G. Louie, *Fundamentals of Condensed Matter Physics* (Cambridge University Press, Cambrige, UK, 2016).

[2] P. Yu and M. Cardona, *Fundamentals of Semiconductors: Physics and Materials Properties*, Graduate Texts in Physics (Springer Berlin Heidelberg, 2010).

[3] P. Misra, *Physics of Condensed Matter* (Elsevier Science, Burlington, USA, 2011).

[4] Atsushi Togo and Isao Tanaka, First principles phonon calculations in materials science, Scr. Mater. **108,** 1 (2015).

[5] J. Fransson, A. M. Black-Schaffer, and A. V. Balatsky, Magnon Dirac materials, Phys. Rev. B **94,** 075401 (2016).

[6] J. O. Vasseur, L. Dobrzynski, B. Djafari-Rouhani, and H. Puszkarski, Magnon band structure of periodic composites, Phys. Rev. B **54,** 1043 (1996).

[7] R. Chisnell, J. S. Helton, D. E. Freedman, D. K. Singh, R. I. Bewley, D. G. Nocera, and Y. S. Lee, Topological Magnon Bands in a Kagome Lattice Ferromagnet, Phys. Rev. Lett. **115,** 147201 (2015).

[8] Barbara Pac, Piotr Petelenz, Andrzej Eilmes, and R. W. Munn, Charge-transfer exciton band structure in the fullerene crystal-model calculations, J. Chem. Phys. **109,** 7923 (1998).

[9] Fengcheng Wu, Fanyao Qu, and A. H. MacDonald, Exciton band structure of monolayer MoS$_2$, Phys. Rev. B **91,** 075310 (2015).

[10] Tawinan Cheiwchanchamnangij and Walter R. L. Lambrecht, Quasiparticle band structure calculation of monolayer, bilayer, and bulk MoS$_2$, Phys. Rev. B **85,** 205302 (2012).

[11] Chi-Cheng Lee, Xiaoqian M. Chen, Yu Gan, Chen-Lin Yeh, H. C. Hsueh, Peter Abbamonte, and Wei Ku, First-principles Method of Propagation of Tightly Bound Excitons: Verifying the Exciton Band Structure of LiF with Inelastic x-Ray Scattering, Phys. Rev. Lett. **111,** 157401 (2013).

[12] R. Daling, W. van Haeringen, and B. Farid, Plasmon dispersion in silicon obtained by analytic continuation of the random-phase-approximation dielectric matrix, Phys. Rev. B **44,** 2952 (1991).

[13] Fabio Caruso, Henry Lambert, and Feliciano Giustino, Band Structures of Plasmonic Polarons, Phys. Rev. Lett. **114,** 146404 (2015).

[14] Walter Stephan, Single-polaron band structure of the Holstein model, Phys. Rev. B **54,** 8981 (1996).

[15] N. Bulut, D. J. Scalapino, and S. R. White, Quasiparticle dispersion in the cuprate superconductors and the two-dimensional Hubbard model, Phys. Rev. B **50,** 7215 (1994).

[16] M. R. Norman, A. H. MacDonald, and Hiroshi Akera, Magnetic oscillations and quasiparticle band structure in the mixed state of type-II superconductors, Phys. Rev. B **51,** 5927 (1995).

[17] Steven G. Johnson and John D. Joannopoulos, *Photonic Crystals: The Road From Theory to Practice* (Springer, New York, NY, 2005).

[18] P. Lalanne, C. Sauvan, and J. P. Hugonin, Photon confinement in photonic crystal nanocavities, Laser. Photon. Rev. **2,** 514 (2008).

[19] W. M. Robertson, G. Arjavalingam, R. D. Meade, K. D. Brommer, A. M. Rappe, and J. D. Joannopoulos, Measurement of Photonic Band Structure in a Two-Dimensional Periodic Dielectric Array, Phys. Rev. Lett. **68,** 2023 (1992).

[20] E. Yablonovitch and T. J. Gmitter, Photonic Band Structure: The Face-Centered-Cubic Case, Phys. Rev. Lett. **63,** 1950 (1989).

[21] Siying Peng, Nick J. Schilder, Xiang Ni, Jorik van de Groep, Mark L. Brongersma, Andrea Alù, Alexander B. Khanikaev, Harry A. Atwater, and Albert Polman, Probing the Band Structure of Topological Silicon Photonic Lattices in the Visible Spectrum, Phys. Rev. Lett. **122,** 117401 (2019).

[22] Tomoki Ozawa, Hannah M. Price, Alberto Amo, Nathan Goldman, Mohammad Hafezi, Ling Lu, Mikael C. Rechtsman, David Schuster, Jonathan Simon, Oded Zilberberg, and Iacopo Carusotto, Topological photonics, Rev. Mod. Phys. **91,** 015006 (2019).

[23] Aaswath Raman and Shanhui Fan, Photonic Band Structure of Dispersive Metamaterials Formulated as a Hermitian Eigenvalue Problem, Phys. Rev. Lett. **104,** 087401 (2010).

[24] Alexey Orlov, Ivan Iorsh, Pavel Belov, and Yuri Kivshar, Complex band structure of nanostructured metal-dielectric metamaterials, Opt. Express **21,** 1593 (2013).

[25] D. V. van Coevorden, R. Sprik, A. Tip, and A. Lagendijk, Photonic Band Structure of Atomic Lattices, Phys. Rev. Lett. **77,** 2412 (1996).

[26] K. M. Ho, C. T. Chan, and C. M. Soukoulis, Existence of a Photonic Gap in Periodic Dielectric Structures, Phys. Rev. Lett. **65,** 3152 (1990).

[27] E. Yablonovitch, T. J. Gmitter, and K. M. Leung, Photonic Band Structure: The Face-Centered-Cubic Case Employing Nonspherical Atoms, Phys. Rev. Lett. **67,** 2295 (1991).

[28] Todd Van Mechelen and Zubin Jacob, Nonlocal topological electromagnetic phases of matter, Phys. Rev. B **99,** 205146 (2019).

[29] Todd Van Mechelen, Sathwik Bharadwaj, Zubin Jacob, and Robert-Jan Slager, Optical *N*-insulators: Topological obstructions to optical Wannier functions in the atomistic susceptibility tensor, Phys. Rev. Res. **4,** 023011 (2022).

[30] Todd Van Mechelen and Zubin Jacob, Viscous Maxwell-Chern-Simons theory for topological electromagnetic phases of matter, Phys. Rev. B **102,** 155425 (2020).

[31] Todd Van Mechelen, Wenbo Sun, and Zubin Jacob, Optical *n*-invariant of graphene's topological viscous Hall fluid, Nat. Commun. **12,** 4729 (2021).

[32] Francesco M. D. Pellegrino, Iacopo Torre, and Marco Polini, Nonlocal transport and the Hall viscosity of two-dimensional hydrodynamic electron liquids, Phys. Rev. B **96,** 195401 (2017).

[33] Todd Van Mechelen and Zubin Jacob, Unidirectional Maxwellian spin waves, Nanophotonics **8,** 1399 (2019).

[34] Todd Van Mechelen and Zubin Jacob, Photonic Dirac monopoles and skyrmions: Spin-1 quantization, Opt. Mater. Express **9,** 95 (2019).

[35] Arthur Mcgurn, *Nanophotonics* (Springer, Cham, Switzerland, 2019).

[36] Siddhant Pandey, Sathwik Bharadwaj, M. Santia, M. Hodek, J. D. Albrecht, and L. R. Ram-Mohan, Cavity electrodynamics with Hermite interpolation: Role of symmetry and degeneracies, J. Appl. Phys. **124,** 213106 (2018).

[37] S. K. Sinha, R. P. Gupta, and D. L. Price, Microscopic theory of dielectric screening and lattice dynamics. I. Local-field corrections and dielectric constants, Phys. Rev. B **9,** 2564 (1974).

[38] Mark S. Hybertsen and Steven G. Louie, Ab initio static dielectric matrices from the density-functional approach. I. Formulation and application to semiconductors and insulators, Phys. Rev. B **35,** 5585 (1987).

[39] Steven G. Louie, James R. Chelikowsky, and Marvin L. Cohen, Local-Field Effects in the Optical Spectrum of Silicon, Phys. Rev. Lett. **34,** 155 (1975).

[40] W. Hanke and L. J. Sham, Many-Particle Effects in the Optical Excitations of a Semiconductor, Phys. Rev. Lett. **43,** 387 (1979).

[41] Stephen L. Adler, Quantum theory of the dielectric constant in real solids, Phys. Rev. **126,** 413 (1962).

[42] Nathan Wiser, Dielectric constant with local field effects included, Phys. Rev. **129,** 62 (1963).

[43] Johannes Flick, Michael Ruggenthaler, Heiko Appel, and Angel Rubio, Atoms and molecules in cavities, from weak to strong coupling in quantum-electrodynamics (QED) chemistry, Proc. Natl. Acad. Sci. **114,** 3026 (2017).

[44] Christian Schäfer, Florian Buchholz, Markus Penz, Michael Ruggenthaler, and Angel Rubio, Making ab initio QED functional(s): Nonperturbative and photon-free effective frameworks for strong light–matter coupling, Proc. Natl. Acad. Sci. **118,** e2110464118 (2021).

[45] Felix Benz, Mikolaj K. Schmidt, Alexander Dreismann, Rohit Chikkaraddy, Yao Zhang, Angela Demetriadou, Cloudy Carnegie, Hamid Ohadi, Bart de Nijs, Ruben Esteban, Javier Aizpurua, and Jeremy J. Baumberg, Single-molecule optomechanics in "picocavities", Science **354,** 726 (2016).

[46] Eleftherios N. Economou, in *The Physics of Solids: Essentials and Beyond* (Springer Berlin Heidelberg, Berlin, Heidelberg, 2010), p. 113.

[47] Alejandro Varas, Pablo García-González, Johannes Feist, F. J. García-Vidal, and Angel Rubio, Quantum plasmonics: From jellium models to ab initio calculations, Nanophotonics **5,** 409 (2016).

[48] Søren Raza, Giuseppe Toscano, Antti-Pekka Jauho, Martijn Wubs, and N. Asger Mortensen, Unusual resonances in nanoplasmonic structures due to nonlocal response, Phys. Rev. B **84,** 121412 (2011).

[49] Mohsen Kamandar Dezfouli, Christos Tserkezis, N. Asger Mortensen, and Stephen Hughes, Nonlocal quasinormal modes for arbitrarily shaped three-dimensional plasmonic resonators, Optica **4,** 1503 (2017).

[50] Owen D. Miller, Ognjen Ilic, Thomas Christensen, M. T. Homer Reid, Harry A. Atwater, John D. Joannopoulos, Marin Soljačć, and Steven G. Johnson, Limits to the optical response of graphene and two-dimensional materials, Nano Lett. **17,** 5408 (2017).

[51] Qiang Zhou, Pu Zhang, and Xue-Wen Chen, General Framework of Canonical Quasinormal Mode Analysis for Extreme Nano-Optics, Phys. Rev. Lett. **127,** 267401 (2021).

[52] René Petersen, Thomas Garm Pedersen, and F. Javier García de Abajo, Nonlocal plasmonic response of doped and optically pumped graphene, MoS_2, and black phosphorus, Phys. Rev. B **96,** 205430 (2017).

[53] H. Frohlich, *Theory of Dielectrics: Dielectric Constant and Dielectric Loss* (Oxford University Press, Oxford, UK, 1990).

[54] J. H. Hannay, The Clausius-Mossotti equation: An alternative derivation, Eur. J. Phys. **4,** 141 (1983).

[55] Pierre Van Rysselberghe, Remarks concerning the Clausius-Mossotti law, J. Phys. Chem. **36,** 1152 (1932).

[56] D. E. Aspnes, Local-field effects effective-medium theory: A microscopic perspective, Am. J. Phys. **50,** 704 (1982).

[57] Marco Govoni and Giulia Galli, Large scale GW calculations, J. Chem. Theory. Comput. **11,** 2680 (2015).

[58] Lars Hedin and Stig Lundqvist, in *Solid State Physics* (Academic Press, Cambridge, MA, USA, 1970), p. 1.

[59] Mark S. Hybertsen and Steven G. Louie, Electron correlation in semiconductors and insulators: Band gaps and quasiparticle energies, Phys. Rev. B **34,** 5390 (1986).

[60] R. Car and Annabella Selloni, Local-Field Effects in the Screening of Impurities in Silicon, Phys. Rev. Lett. **42,** 1365 (1979).

[61] Serdar Öğüt, Russ Burdick, Yousef Saad, and James R. Chelikowsky, Ab Initio Calculations for Large Dielectric Matrices of Confined Systems, Phys. Rev. Lett. **90,** 127401 (2003).

[62] M. Gajdoš, K. Hummer, G. Kresse, J. Furthmüller, and F. Bechstedt, Linear optical properties in the projector-augmented wave methodology, Phys. Rev. B **73,** 045112 (2006).

[63] Gianluca Prandini, Mario Galante, Nicola Marzari, and Paolo Umari, Simple code: Optical properties with optimal basis functions, Comput. Phys. Commun. **240,** 106 (2019).

[64] A. K. Rajagopal, Longitudinal transverse dielectric functions of a two-dimensional electron system: Inclusion of exchange correlations, Phys. Rev. B **15,** 4264 (1977).

[65] A. K. Rajagopal and K. P. Jain, Orbital susceptibility of an interaction electron gas, Phys. Rev. A **5,** 1475 (1972).

[66] R. Del Sole and E. Fiorino, Macroscopic dielectric tensor at crystal surfaces, Phys. Rev. B **29,** 4631 (1984).

[67] See Supplemental Material at http://link.aps.org/supplemental/10.1103/PhysRevApplied.18.044065 for a detailed derivation of the atomistic longitudinal and transverse dielectric functions, solutions to the picophotonic nonlinear eigenvalue equation in silicon, and the total transmission coefficient in silicon including contributions from both regular and anomalous bands.

[68] Lars Jönsson, Zachary H. Levine, and John W. Wilkins, Large Local-Field Corrections in Optical Rotatory Power of Quartz and Selenium, Phys. Rev. Lett. **76,** 1372 (1996).

[69] M. V. Berry, in *Anomalies, Phases, Defects–Ferrara, June 1989*, Monographs and Textbooks in Physical Science, edited by M. Bregola, G. Marmo, and G. Morandi (Bibliopolis, Naples, Italy, 1990) Chapter 3, p. 125.

[70] David Linton Johnson, Local-field effects x-ray diffraction the possibility of observing the optical Borrmann effect: Solutions to Maxwell's equations in perfect crystals, Phys. Rev. B **12**, 3428 (1975).

[71] Marvin L. Cohen and T. K. Bergstresser, Band structures and pseudopotential form factors for fourteen semiconductors of the diamond and zinc-blende structures, Phys. Rev. **141**, 789 (1966).

[72] Prashant Shekhar, Marek Malac, Vaibhav Gaind, Neda Dalili, Al Meldrum, and Zubin Jacob, Momentum-resolved electron energy loss spectroscopy for mapping the photonic density of states, ACS Photonics **4**, 1009 (2017).

[73] Prashant Shekhar, Sarang Pendharker, Harshad Sahasrabudhe, Douglas Vick, Marek Malac, Rajib Rahman, and Zubin Jacob, Extreme ultraviolet plasmonics and Cherenkov radiation in silicon, Optica **5**, 1590 (2018).

[74] Wayne M. Saslow and George F. Reiter, Plasmons and characteristic energy loss in periodic solids, Phys. Rev. B **7**, 2995 (1973).

[75] John P. Walter and Marvin L. Cohen, Wave-vector-dependent dielectric function for Si, Ge, GaAs, and ZnSe, Phys. Rev. B **2**, 1821 (1970).

[76] John P. Walter and Marvin L. Cohen, Frequency and wave-vector dependent dielectric function for silicon, Phys. Rev. B **5**, 3101 (1972).

[77] David R. Penn, Wave-number-dependent dielectric function of semiconductors, Phys. Rev. **128**, 2093 (1962).

[78] G. Srinivasan, Microscopic dielectric function of a model semiconductor, Phys. Rev. **178**, 1244 (1969).

[79] Prabha Sharma and Sushil Auluck, Wave-vector-dependent dielectric function for a model semiconductor, Phys. Rev. B **23**, 874 (1981).

[80] Charles. Kittel, *Introduction to Solid State Physics* (J. Wiley, Hoboken, NJ, 2005), 8th ed.

[81] H. R. Philipp and H. Ehrenreich, Optical properties of semiconductors, Phys. Rev. **129**, 1550 (1963).

[82] D. H. Reitze, T. R. Zhang, Wm M. Wood, and Michael C. Downer, Two-photon spectroscopy of silicon using femtosecond pulses at above-gap frequencies, JOSA B **7**, 84 (1990).

[83] Gary F. Sinclair, Nicola A. Tyler, Döndü Sahin, Jorge Barreto, and Mark G. Thompson, Temperature Dependence of the Kerr Nonlinearity and Two-Photon Absorption in a Silicon Waveguide at $1.55 \ \mu$m, Phys. Rev. Appl. **11**, 044084 (2019).

[84] Stephen Jesse, Albina Y. Borisevich, Jason D. Fowlkes, Andrew R. Lupini, Philip D. Rack, Raymond R. Unocic, Bobby G. Sumpter, Sergei V. Kalinin, Alex Belianinov, and Olga S. Ovchinnikova, Directing matter: Toward atomic-scale 3D nanofabrication, ACS Nano **10**, 5600 (2016).

[85] Ondrej Dyck, Maxim Ziatdinov, David B. Lingerfelt, Raymond R. Unocic, Bethany M. Hudak, Andrew R. Lupini, Stephen Jesse, and Sergei V. Kalinin, Atom-by-atom fabrication with electron beams, Nat. Rev. Mater. **4**, 497 (2019).

[86] Alexander M. Jakob, Simon G. Robson, Vivien Schmitt, Vincent Mourik, Matthias Posselt, Daniel Spemann, Brett C. Johnson, Hannes R. Firgau, Edwin Mayes, Jeffrey C. McCallum, Andrea Morello, and David N. Jamieson, Deterministic shallow dopant implantation in silicon with detection confidence upper-bound to 99.85% by ion–solid interactions, Adv. Mater. **34**, 2103235 (2022).

[87] R. F. Sabiryanov and S. S. Jaswal, Magneto-optical properties of MnBi and MnBiAl, Phys. Rev. B **53**, 313 (1996).

[88] J. Stiebling and H. Raether, Dispersion of the Volume Plasmon of Silicon (16.7 eV) at Large Wave Vectors, Phys. Rev. Lett. **40**, 1293 (1978).